Electronic Supplementary Material (ESI) for Nanoscale.

Synthesis, Optical Properties and Theoretical Modelling of Discrete Emitting States in Doped Silicon Nanocrystals for Bioimaging

B. F. P. McVey,[a b c] D. König, [d e] X. Cheng,[a c] P. B. O'Mara,[a c] P. Seal,[d e] X. Tan, [d e] H. A. Tahini,[d e] S. C. Smith, [d e] J. J. Gooding, [a c f] R. D. Tilley[a b c*]*

[a] School of Chemistry, [b] Electron Microscopy Unit Mark Wainwright Analytical Centre, [c] Australian Centre for Nanomedicine, [d] School of Chemical Engineering, [e] Integrated Materials Design, [f] ARC Centre of Convergent Bio-Nano Science and Technology, University of New South Wales, Sydney, NSW 2052, Australia. * = denotes corresponding authors

E-mail: r.tilley@unsw.edu.au.

solidstatedirk@gmail.com

Experimental Section

Synthesis, surface passivation, and purification of undoped and Cu doped Si NCs

Undoped silicon nanocrystals were synthesized according to procedures detailed by Shiohara *et al*[1]

Cu doped Si NCs were synthesized using an identical method to undoped Si NCs, except for the amount of dopant precursor added. Anhydrous Cu(II) chloride is extremely moisture sensitive, and therefore was stored in a nitrogen filled glovebox. For 2 Cu dopants per NC 0.0136 mmol (0.0017 g) of anhydrous Cu(II) chloride was added. For 4 Cu dopants per 0.0272 mmol (0.0035 g) of anhydrous Cu(II) chloride was added. For 6 Cu dopants per NC 0.0544 mmol (0.0070 g) of $CuCl_2$ (99 %, *Sigma Aldrich*) was added. Inside a nitrogen filled glovebox dopant precursors are added concurrently with tetroctylammonium bromide.

In a typical surface passivation reaction, a quartz tube was attached to a Schlenk line and was degassed by three cycles of evacuation and purging with argon for up to 5 minutes per cycle. Hydride capped undoped or metal doped silicon nanocrystals were then transferred via a degassed syringe from the Schlenk tube to the quartz tube. 3 mL of degassed allylamine (99 %, *Sigma Aldrich*) was then added to the mixture, the tube was then exposed to UV light (254 nm) for four hours, producing alkylamine capped undoped or Cu doped Si NCs.

Undoped Si NCs were purified by column chromatography. Purification of Cu doped Si NCs involved a two-step process, including column chromatography and washing with a metal removing agent, bipyridine.

For column chromatography unpurified alkylamine capped undoped or Cu doped Si NCs were transferred to a round bottom flask and the solvent was removed under reduced pressure. 20 mL of MilliQ water was added to the unpurified NCs and the mixture was dispersed via ultrasonic

sonication for 5 minutes producing a cloudy white solution, which was filtered by using Millipore 0.45 μm filter paper. The filtrate was then concentrated down to 2-3 mL (yellow oily appearance) via reduced pressure and then put into a size exclusion column (φ = 1 cm, 60 cm) with Sephadex LH-20 beads (*GE Lifesciences*) (bead size 25 – 100 μm) acting as the stationary phase and MilliQ water as the solvent. Size exclusion chromatography is the first purification procedure, which has been shown to highly successful at removal of surface bound metal dopants. The flow rate used was 1 drop every 5 seconds and fractions were collected in an automated test tube collector with test tubes set to cycle every 8 minutes. Fractions collected were checked for luminescence via the use of a handheld UV light (365 nm). Fractions that displayed luminescence were combined and concentrated under reduced pressure to yield purified undoped or Cu doped Si NCs (light yellow oil).

Before characterization Cu doped Si NCs were further purified *via* washing with bipyridine. Bipyridine has been shown as an effective solvent for the removal of low/zero valent metals from nanocrystal surfaces. A 50 times excess of bipyridine was added to Cu doped Si NCs dispersed in tetrahydrofuran. This mixture was then sonicated for 10 minutes and left to stir for 1 hour. Cu doped Si NCs were then subject to column purification to remove excess bipyridine.

Structural and optical characterization of undoped and Cu doped Si NCs

For TEM, a small drop of a highly concentrated (15-20 mg/mL) NC solution was drop cast onto a formvar coated gold grid. The grid was left to slowly evaporate in ambient conditions. The TEM used was a Phillips cm200 operated at 200 kV.

ICP-MS measurements were carried out at the Mark Wainwright Analytical Centre, University of New South Wales. Preparation for ICP-MS involved producing a dilute solution of purified Cu doped silicon nanocrystals in MilliQ water (0.5 mg/mL).

For absorption measurements, NCs were dispersed in MilliQ water with concentrations between 1-5 mg/mL. Absorption measurements were carried out on a Cary 50 UV-Vis spectrometer. Blank measurements were carried out using MilliQ water. For absorption coefficient calculations the method developed by Hessel *et al*[2] was used.

For emission measurements, undoped and Cu doped Si NCs had identical concentrations to absorption measurements. Emission measurements were recorded on a Shimadzu RF-5301PC spectrofluorophotometer using an excitation and emission slit width of 5 mm.

Fluorescent quantum yields were calculated using the comparative method. The quantum yield standard used was quinine sulfate. All tested nanocrystals had an optical density between 0.05 - 0.17 at the excitation wavelength used.

Density Functional Calculations

DFT computations were carried out with nonperiodic boundary conditions using the GAUSSIAN09 program package. [3] We computed NC approximants by real space DFT methods to allow for an investigation of Cu doping unperturbed by effects of periodic boundary conditions such as wave function overlaps due to an adjacent system in the immediate proximity. As DFT computation route, we used the Hartree-Fock (HF) method for structural optimisation where the exact exchange interaction inherent to HF is crucial in obtaining accurate bond geometries with peak and RMS force limits of 450 and 300 μHa, respectively. Optimised geometries were subject to electronic structure calculation with the B3LYP hybrid DF,[2-3] accounting for local and non-local exchange and correlation interaction. As all-electron molecular orbital (MO) basis set (BS) we used the Karlsruhe default2-single-ξ valence MO-BS with d-polarization functions (def2-SZVP).[4] During all calculations, no symmetry constraints were applied to the MOs and tight convergence criteria with ultrafine integration grids were used in the self-consistent field routine. The above computation route has been experimentally proven to deliver very accurate results for Si NC systems.[3-6]

Cytotoxicity and Bioimaging experiments

For cytotoxicity tests 20 μL of purified alkylamine passivated Cu doped Si NCs (2 or 6 dopants per NC) or undoped Si NCs were added to a 96 well plate cultured with HeLa cells and incubated for 24 hours. After incubation, the MTT reagent (3-[4,5-dimethylthiazol-2-yl]-2,5-diphenyltetrazolium bromide) (5 mg/mL) was reconstituted in phosphate buffer solution (PBS)

and added to each well in an equal volume. The absorption measurements were performed using a FLUOstar fluorescence plate reader (BMG Labtech) at 570 nm and background at 690 nm.

For *in vitro* imaging HeLa cells were fluorescently labeled using alkylamine passivated Cu doped silicon nanocrystals (6 dopants per NC) or undoped silicon nanocrystals. Cells were cultured in a 75 cm^2 incubation flask with ~12 mL of medium (500 mL of Dulbecco's modified Eagle's medium (DMEM), 10% fetal calf serum, and 4 mmol l-glutamine). At 1 day prior to the imaging, the cells were plated at a density of ~50 000/plate in a Petri dish with 2 mL of medium. On the day of imaging, cells were grown to at least 80% confluence. To allow uptake of Cu doped and undoped silicon nanocrystals, nanocrystal dispersion in 1× PBS was added to the medium to reach a final concentration of 50–100 μg/mL before further incubating the cells at 37 °C for 2–3 hours. Immediately before imaging, the medium was removed and cells were carefully washed 3 times with fresh PBS solution. The cells were imaged using a Zeiss Axiovert 200 M under total internal reflectance reflection fluorescence (TIRF) imaging mode.

SI Table 1 - Raw ICP-MS values

Sample	**Cu (micrograms)**	**Cu (mmol)**
$Cu_{1-x}Si_x$ (2 Cu dopants)*	**25.6 ± 2.0**	**1.61 ± 0.12**
$Cu_{1-x}Si_x$ (4 Cu dopants)*	**61.1 ± 2.0**	**3.88 ± 0.12**
$Cu_{1-x}Si_x$ (6 Cu dopants)*	**92.7 ± 2.0**	**5.89 ± 0.12**

SI Table 1 Mass of Copper metal detected in each sample via ICP-MS. * responds to an average number of dopants per nanocrystal.

SI Figure 1 – Histograms of undoped and Cu doped Si NCs (2 dopants per NC)

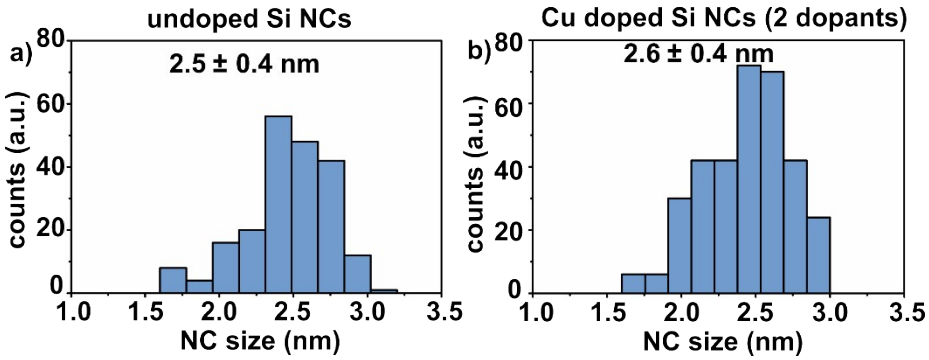

SI Figure 1: a) and b) contain histograms of measured nanocrystal sizes for undoped Si NCs and Cu doped Si NCs at a dopant concentration of 2 Cu dopants per NC.

SI Figure 2 – TEM and histograms of Cu doped Si NCs (4 and 6 dopants per NC)

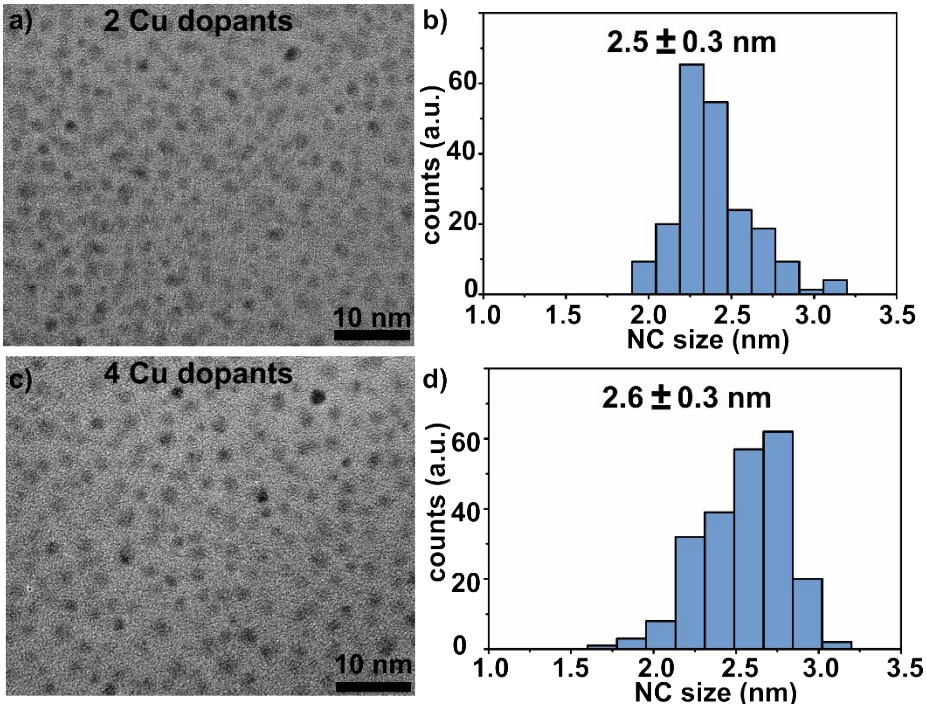

SI Figure 2: a) and b) contain transmission electron microscopy images of Cu doped Si NCs at dopant concentrations of 4 and 6 Cu dopants per NC. c) and d) contain histograms of measured NC sizes for Cu doped Si NCs at dopant concentrations of 4 and 6 Cu dopants per NC.

SI Figure 3 – FTIR of undoped and Cu doped Si NCs (2, 4, and 6 dopants per NC)

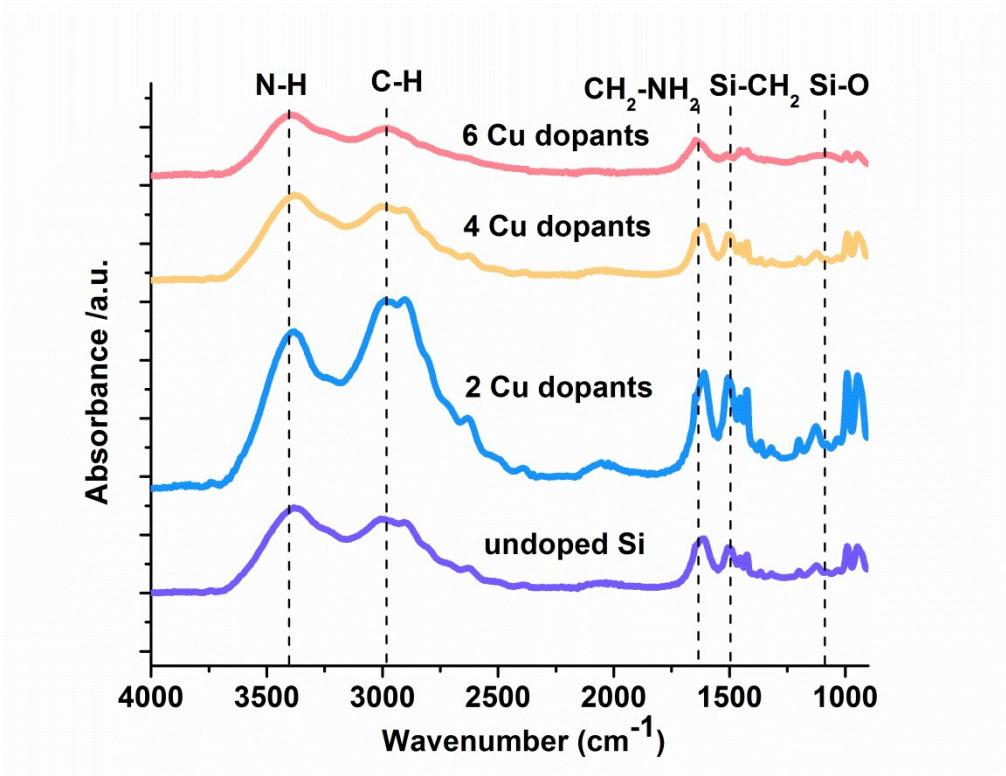

SI Figure 3: FTIR spectra of undoped Si NCs and Cu doped Si NCs at dopant concentrations of 2, 4, and 6 dopants per NC. Both undoped and Cu doped Si NCs have been functionalized with allylamine via UV assisted hydrosilylation.

SI Figure 4 – H^1 NMR of Cu doped Si NCs (2 dopants per NC)

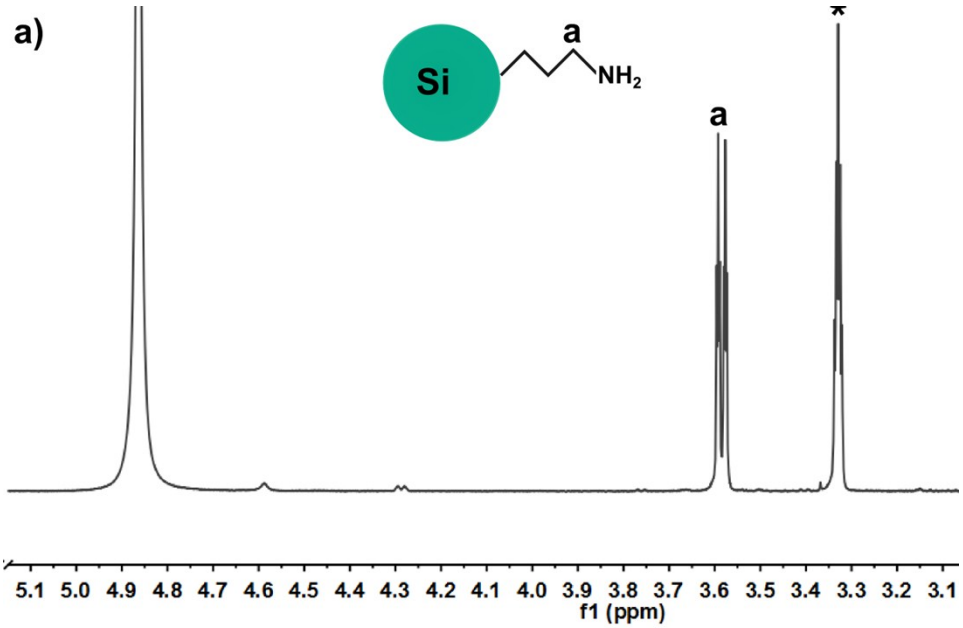

SI Figure 4: H^1 NMR of Cu doped Si NCs at dopant concentrations of 2 dopants per NC. The Asterisk

SI Table 2 – Absorption coefficients of undoped and Cu doped Si NCs (6 dopants per NC)

Wavelength	488 nm	400 nm	350 nm	330 nm
Undoped Si absorption coefficients ($L\ cm^{-1}\ mol^{-1}$)	1.0×10^4	2.1×10^4	3.7×10^4	8.1×10^4
Cu doped Si absorption coefficients ($L\ cm^{-1}\ mol^{-1}$)	1.5×10^4	5.9×10^4	8.6×10^5	1.1×10^5

SI Figure 5 – Emission data for undoped and Cu doped Si NCs

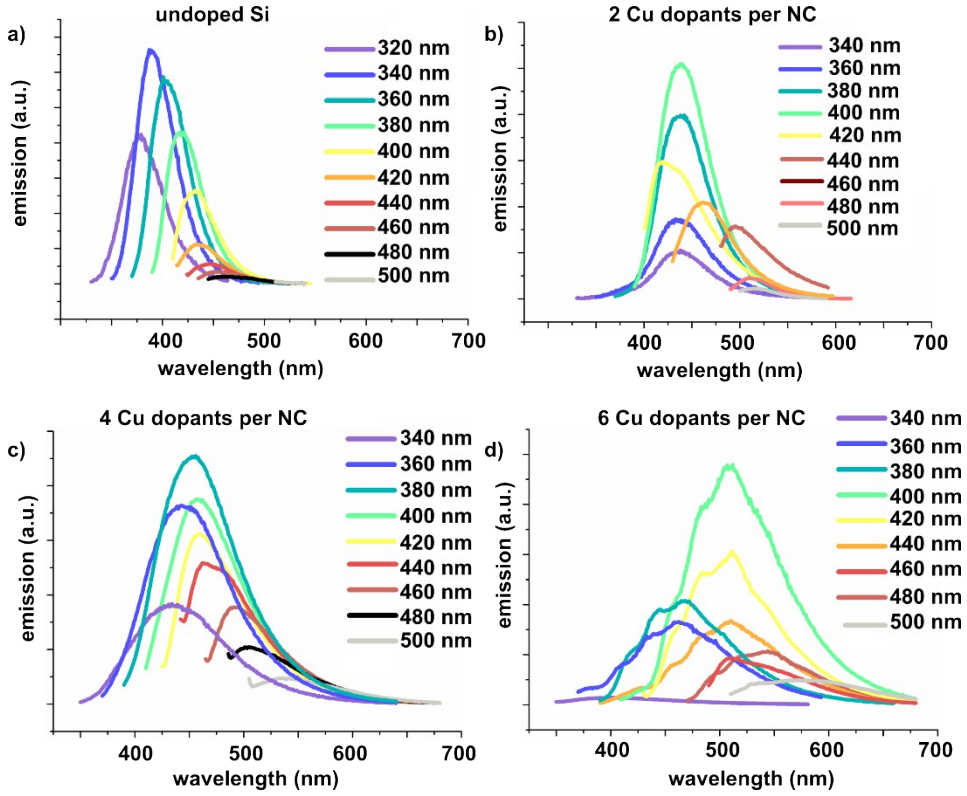

SI Figure 5: Full emission spectra of a) undoped Si NCs b), c), and d) contain full emission spectra of Cu doped Si NCs at dopant concentrations of 2, 4, and 6 dopants per NC.

SI Figure 6 – Fits of emission data for undoped and Cu doped Si NCs

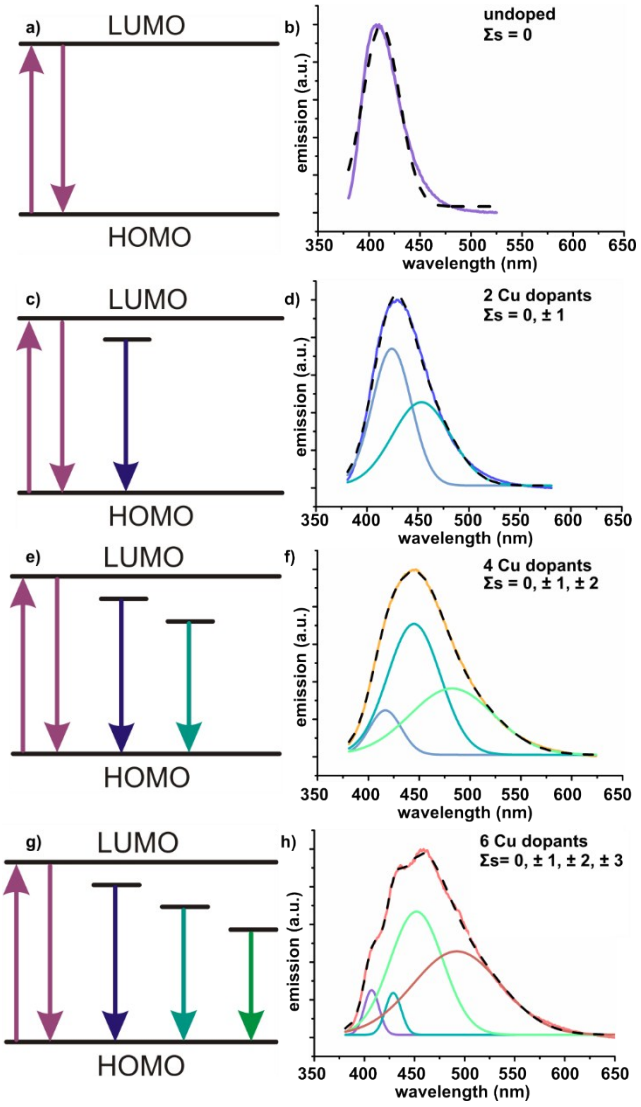

SI Figure 6 a), c), e), g) Scheme highlighting the newly introduced pathways caused by spin-orbit coupling of Cu atoms in doped Si NCs. The up and down arrows show excitation and emission. b), d), f), h) experimental emission spectra for undoped and Cu doped Si NCs at dopant concentrations of 2, 4, and 6 dopants per NC. The fits are added to the emission spectra highlighting the formation of multiple emission pathways by Cu dopants.

SI Figure 7 – raw quantum yield data

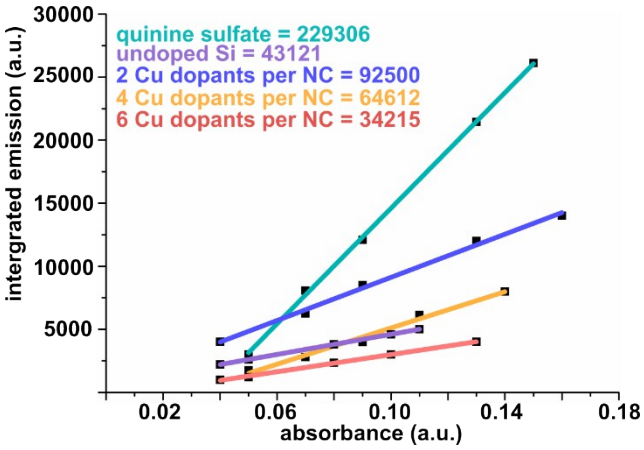

SI Figure 7: raw quantum yield data of undoped Si NCs, Cu doped Si NCs at all dopant concentrations tested, and standard (quinine sulfate).

SI Figure 8 – Full scheme of spin-orbit coupling model

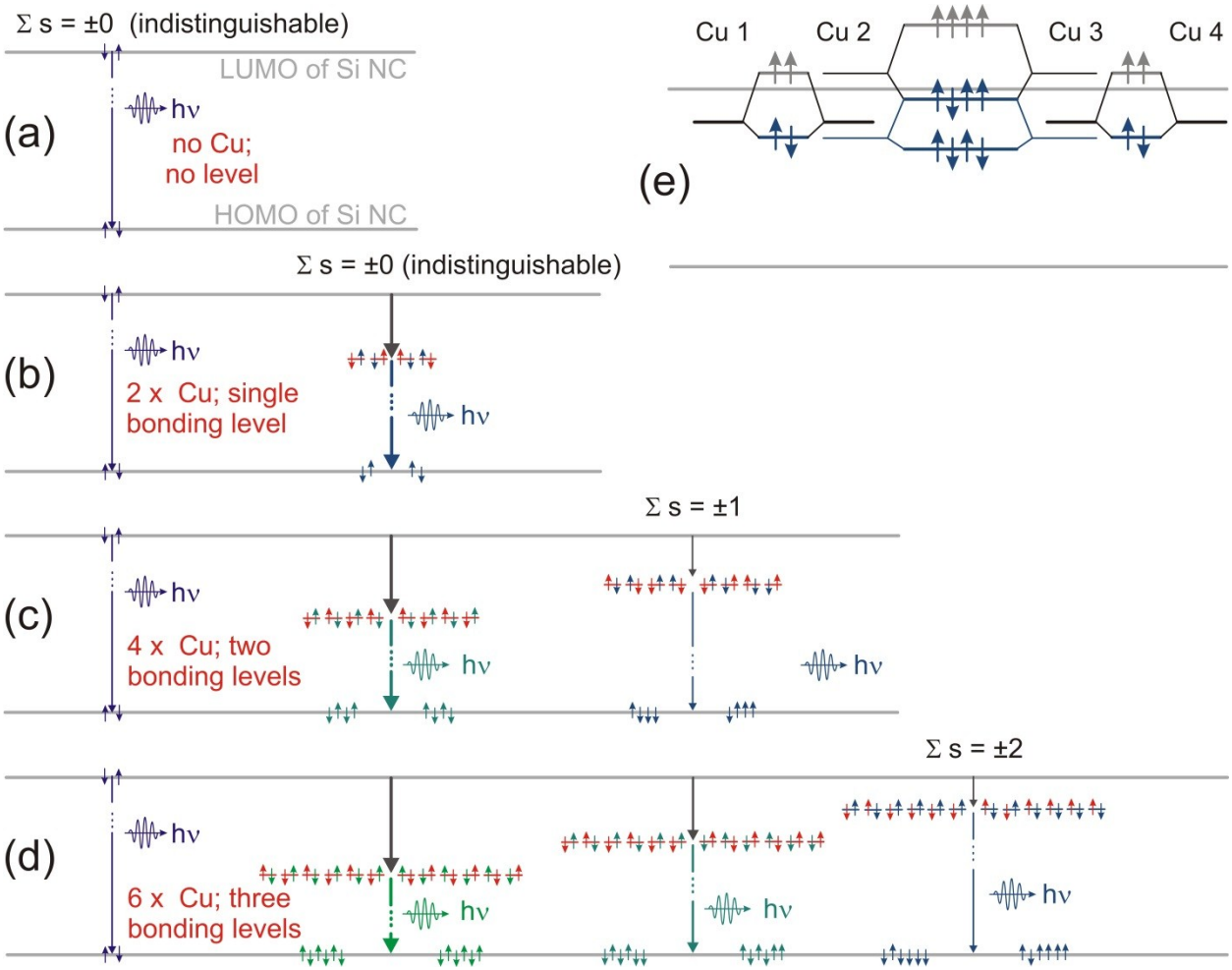

SI Figure 8: Energy configuration scheme of interstitial Cu 4s1 states determined by exchange interaction in compound with spin multiplet orientation. Undoped Si NCs with default singlet transitions (a). Adding 2 Cu atoms results in singly occupied energy levels within the HOMO-LUMO gap of undoped NC; only bonding MOs shown here. Red arrows show unoccupied states, arrow direction accounts for spin orientation which split up in accord with spin selection rules, providing two singlet states with one Cu-associated energy level for 2 Cu interstitials (b), four quadruplet states with two Cu-associated energy levels for 4 Cu interstitials (c), and six sextet states with three Cu-associated energy levels for 4 Cu interstitials (d). The sum of spins (Σs) per

Cu atom is given on the top of the energy diagrams for each Cu-associated energy level. Blue to green arrows in HOMO level of Si NC present allowed final spin states of radiative transitions which are shown by photon (hν) emission seen in PL, emission symbols are placed at lowest energy process; coloured arrows correspond to colour of emitted hν. The four radiative transitions of Si NCs with 6 Cu interstitials correspond to the four sub-peaks in PL for six Cu dopants in SI Figures 5g and h. Hückel diagram of the formation of HOMOs within the fundamental NC gap derived from hybridization of Cu-4s1-associated MOs (e), shown for two Cu atoms in one NC (left, right) and further development of hybridization with four Cu atoms within one NC. Anti-bonding Cu-4s1-associated MOs (grey) are located within the anti-bonding electronic DOS (unoccupied MOs – UMOs) and therefore do not introduce additional optical transitions at energies within the fundamental gap of the undoped Si NC.

SI Figure 9 – Electron DOS graph for $Si_{84}(CH_3)_{64}$ Cu doped Si NCs (2 dopants per NC)

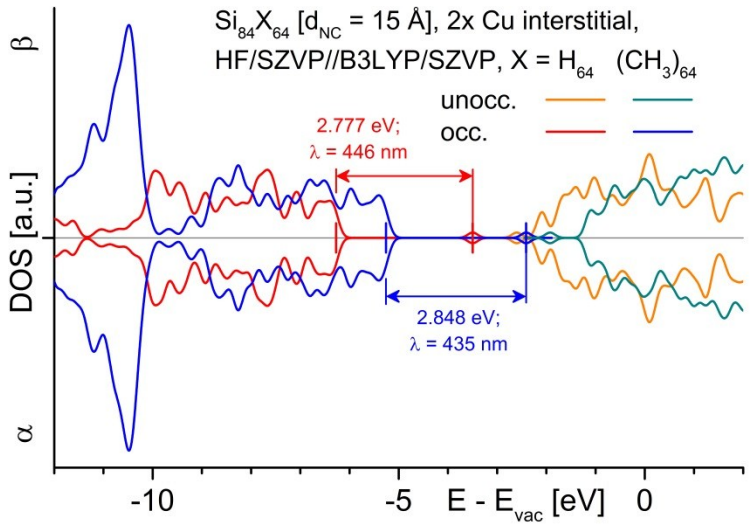

SI Figure 9: Electronic DOS over energy relative to vacuum level E_{vac} of $Si_{84}(CH_3)_{64}$ and $Si_{84}H_{64}$ NC approximants (1.5 nm size), both doped with 2x Cu at corner position, see Figure S-B. The difference in radiative energy transition of 2.6 % relative (0.071 eV absolute) justifies the replacement of full CH_3- by full H-termination to keep DFT calculations of Si_{286} NC approximants (2.3 nm size) tractable. A shift of the entire electronic DOS towards higher binding energies for full CH_3-termination of about 1.0 eV is due to the difference in interface charge transfer from the NC core (Si) to the respective interface termination, see references (1) to (3).

SI Figure 10 – DFT generated picture of Cu dopant molecular orbitals (methyl and hydride terminated clusters)

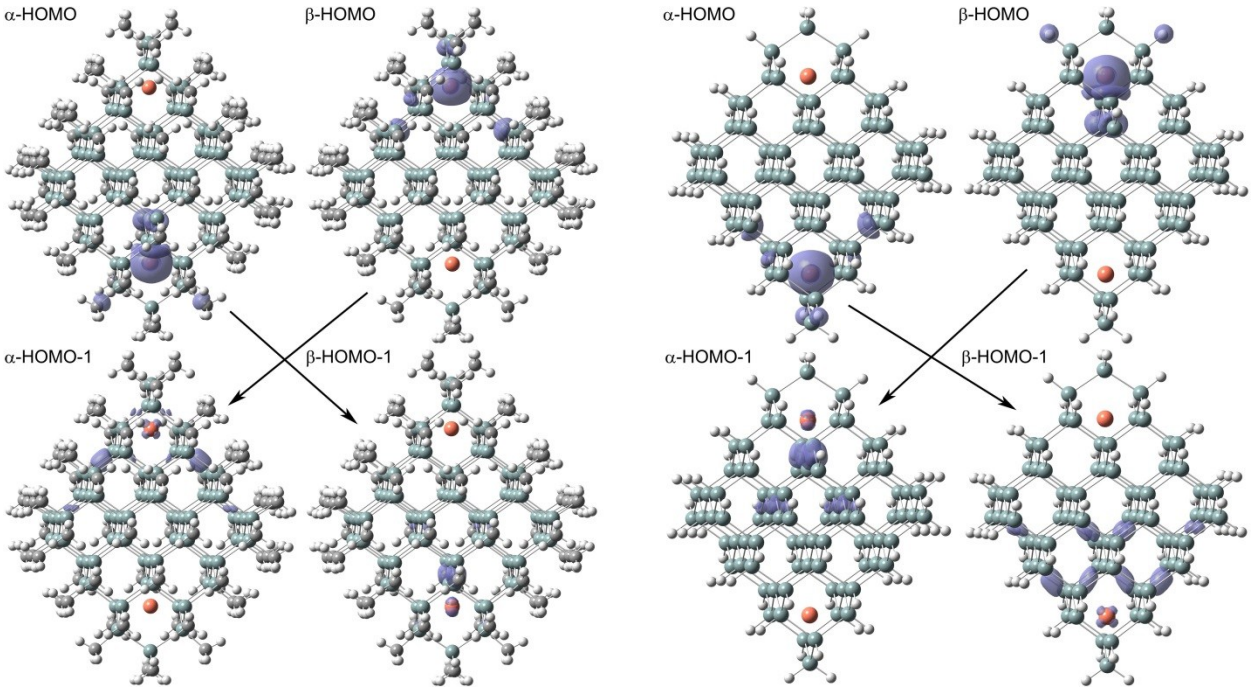

SI Figure 10: Densities of MOs relevant for visible optical transition involving interstitial Cu atoms for $Si_{84}(CH_3)_{64}$ approximants (left) and $Si_{84}H_{64}$ approximants (right). Arrows indicate photon emission paths. Allowed radiative transitions involve an integer change in spin quantum number (spin flip) due to the bosonic nature of photons, resulting in decay paths $\alpha \rightarrow \beta$ and $\beta \rightarrow \alpha$. The spatial separation of initial and final states defining the radiative transition is not as pronounced as for Si_{286} NCs (2.3 nm size, see Figures 4 in main publication) due to smaller NC size. Iso-surface plots encompass areas with MO state density of $\geq 1.5\times10^{-3}$ $e/a_{B,0}$ (10 e/nm^3).

SI Figure 11 – DFT generated picture of undoped Si molecular orbitals (methyl and hydride terminated clusters)

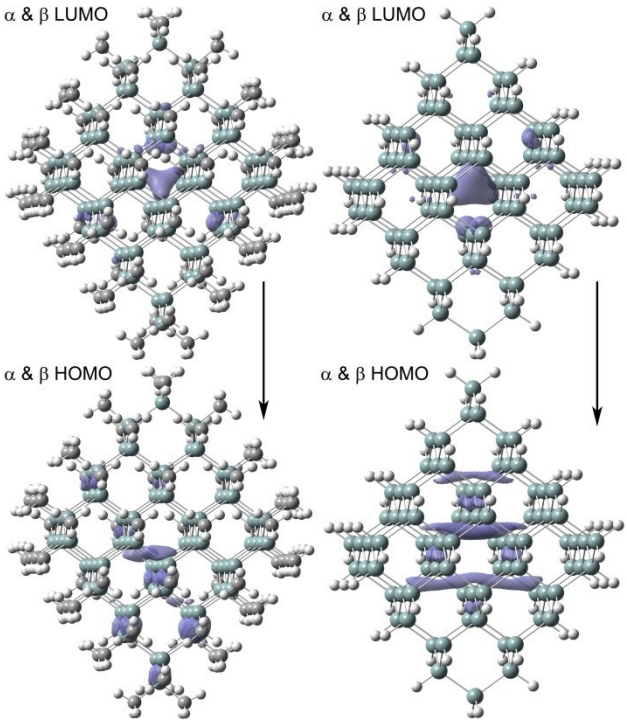

SI Figure 11: Densities of MOs relevant for visible optical transition of nominal (undoped) $Si_{84}(CH_3)_{64}$ approximant (left) and $Si_{84}H_{64}$ approximant (right). Arrows indicate photon emission paths. Since all MOs are either fully occupied or fully unoccupied, no spin selection rules apply to optical transitions (spin singlet), and MO densities present both, α and β spin orientations. Iso-surface plots encompass areas with MO state density of $\geq 7.5\times10^{-4}$ $e/a_{B,0}$ (5 e/nm^3).

SI Figure 12 – Electron DOS graph for $Si_{84}(CH_3)_{64}$ undoped Si NCs (2 dopants per NC)

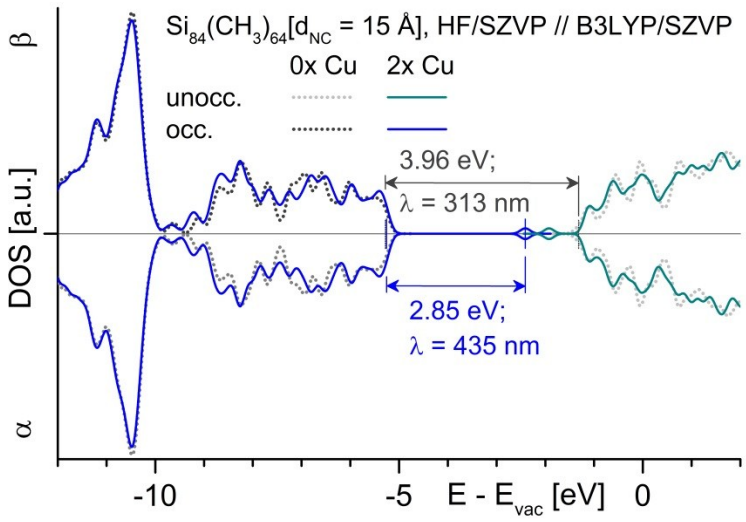

SI Figure 12: Electronic DOS over energy relative to vacuum level E_{vac} of nominal (undoped) $Si_{84}(CH_3)_{64}$ approximant and and $Si_{84}(CH_3)_{64}$ approximant doped with 2 Cu atoms at interstitial positions near NC corners, see Figures Si-B (left) and Si-C (left); NC size is 1.5 nm. Transition energies align to trend of increased quantum confinement and relative energy difference between fundamental gap and Cu-induced optical transitions.

SI Figure 13 – Results from MTT assay

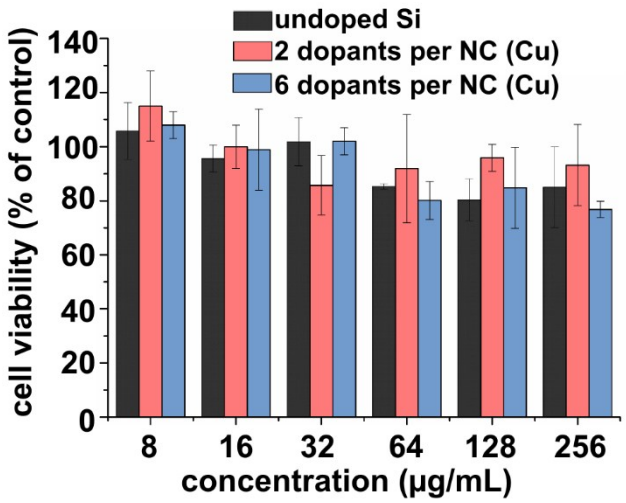

MTT assay of undoped and Cu doped Si NCs incubated with HeLa cells. For the Cu doped silicon nanocrystals two concentrations were chosen to see the effect of dopant concentration on cytotoxicity (2 or 6 Cu dopants per nanocrystal). Cell viability is expressed as percentage of control (control = HeLa cells with no silicon nanocrystals).

References

1) A. Shirohara, S. Prabakar, A. Faramus, C-Y, Hsu, P-S, Lai, P. T. Northcote, R. D. Tilley, *Nanoscale* **2011**, *3*, 3364-3370.

2) C. M. Hessel, D. Reid, M. G. Pathani, M. R. Rasch, B. W. Goodfellow, J. Wei, H. Fuji, V. Ahkvan, B. A. Korgel, *Chem. Mater*. **2012**, *24*, 393-401.

3) D. König, J. Rudd, M. A. Green, G, Conibeer, *Phys. Rev. B* **2008**, *78*, 035339.

4) D. König, J. Rudd, M. A. Green, G, Conibeer, *Solar Energy Mater. & Solar Cells* **2009**, *93*, 753-758

5) D. König, D. Hiller, S. Gutsch, M. Zacharias, *Adv. Mater. Interfaces* **2014**, *1*, 1400359.

6) D. Hiller, J. Lopéz-Vidrier, S. Gutsch, M. Zacharias, M. Wahl, W. Bock, A. Brodyanski, M. Kopnarski, K. Nomoto J. Valenta, D. König, *Sci. Reports* **2017** 8337.